Journal of Drug Delivery Science and Technology 110 (2025) 107098

Contents lists available at ScienceDirect

Journal of Drug Delivery Science and Technology

journal homepage: www.elsevier.com/locate/jddst

Harnessing nanoencapsulation for the repurposing of hydroquinidine against breast cancer

Turan Demircan [a,*], Daela Milinkovic [b], Esin Sakallı Çetin [a], Ebrunur Aksu [c], Oya Tagit [b,**]

[a] Muğla Sıtkı Koçman University, Faculty of Medicine, Medical Biology Department, Mentese, 48100, Muğla, Türkiye
[b] FHNW University of Applied Sciences and Arts Northwestern Switzerland, Institute of Chemistry and Bioanalytics, Group of Biointerfaces, Muttenz, Switzerland
[c] Muğla Sıtkı Koçman University, Institute of Health Sciences, Medical Biology Department, Mentese, 48100, Muğla, Türkiye

ARTICLE INFO

Keywords:
Hydroquinidine
Breast cancer
PLGA nanoparticles
Drug delivery
Anticancer efficacy
Nanoencapsulation

ABSTRACT

Repurposing drugs beyond their original medical indications can facilitate cost- and time-effective drug development and a sustainable drug development process. Nanoencapsulation strategies can further expand the number of potentially suitable drug candidates for repurposing. In this study, we explored the anticancer efficacy of hydroquinidine (a class IA antiarrhythmic cinchona alkaloid drug) loaded into PLGA nanoparticles (HQ-NP) on breast cancer cells. The study compared HQ-NP to soluble hydroquinidine (HQ_{sol}) in estrogen receptor-positive MCF7 and triple-negative MDA-MB-231 breast cancer cell lines. Overall, nanoencapsulation resulted in more potent and selective toxicity in comparison to soluble drug. The mechanisms involved inducing apoptosis and oxidative stress, disruption of mitochondrial membrane potential, and suppression of cell proliferation. The enhanced potency of HQ-NP was consistent across multiple assays and on both cell lines, suggesting a broad applicability in different breast cancer subtypes. *In silico* analyses indicated the cancer-related pathways, such as PI3K-Akt and cAMP signaling, as potential targets of HQ, which is likely to be driven by the putative inhibition of voltage-gated ion channels as suggested by molecular docking studies. This research highlights the potential of HQ-NP as a novel, multi-modal anticancer agent for breast cancer treatment, warranting further investigation towards clinical application.

1. Introduction

Cancer remains one of the leading causes of mortality worldwide, demanding continued research into the discovery and development of novel therapeutic agents. Identifying new therapeutic potential of existing drugs beyond their original medical indication, so-called drug repurposing (or repositioning), is a promising approach for cost- and time-effective drug development [1]. Leveraging the established knowledge of the drug safety profiles, drug repurposing can significantly reduce development costs, shorten timelines, and simplify regulatory approval procedures [2], leading to a more sustainable drug development process. The efficiency of repositioned drugs is strictly evaluated by their side effects and resistance profiles [1]. As the physicochemical characteristics of drugs are tailored to the requirements of originally intended diseases, repurposing these drugs for other indications often requires new formulation and delivery methods to maximize their efficacy and safety profiles. The risks of poor solubility, sub-optimal accumulation and bioavailability in tumors, rapid clearance, and off-target toxicity of drugs repositioned against cancer can be addressed by formulating and delivering them as nanoparticles (NPs) [3]. Improved tumor accumulation, sustained release profiles, and reduced systemic toxicity have been reported for various types of nanoencapsulated drugs compared to their free drug counterparts [4]. Moreover, nanoparticle-based delivery systems protect drugs from premature degradation and can overcome multidrug resistance mechanisms often encountered in cancer cells. NP-based formulations can also allow for customization of pharmacokinetics and biodistribution, as well as targeted delivery to the new cellular and molecular targets [5], expanding the range of suitable drug candidates for cancer treatment.

Hydroquinidine (HQ), a class IA antiarrhythmic cinchona alkaloid drug [6], has long been utilized in managing ventricular arrhythmias via blocking the fast sodium channels [7]. Recently, we have demonstrated the effects of HQ on lung, colon, and liver cancer models. Notably, HQ could induce apoptosis, inhibit cell proliferation, and modulate key

* Corresponding author.
** Corresponding author.
E-mail addresses: turandemircan@mu.edu.tr (T. Demircan), oya.tagit@fhnw.ch (O. Tagit).

https://doi.org/10.1016/j.jddst.2025.107098
Received 7 November 2024; Received in revised form 29 April 2025; Accepted 26 May 2025
Available online 26 May 2025

signaling pathways linked to cancer progression [8–10]. The mechanism of action involves multiple targets, such as modulation of potassium signaling [11], which facilitates its broad-spectrum anticancer activity. However, HQ is associated with poor aqueous solubility and gastrointestinal side effects upon oral administration [12]. Therefore, repositioning HQ for cancer therapy could greatly benefit from nanoencapsulation strategies, which we explore in this study for breast cancer.

The highly heterogeneous nature of breast cancer demands diverse treatment approaches, as different molecular subtypes exhibit varying responses to therapies. Two widely studied breast cancer cell lines, MCF-7 and MDA-MB-231, represent distinct molecular profiles and are frequently used in preclinical research to evaluate potential anticancer agents [13]. MCF-7 cells are characterized by their estrogen receptor (ER) positivity, making them responsive to hormonal therapies and representative of luminal A breast cancers [14]. In contrast, MDA-MB-231 cells are triple-negative, lacking expression of ER, progesterone receptor (PR), and human epidermal growth factor receptor 2 (HER2) [15]. This triple-negative phenotype is associated with more aggressive disease and limited targeted therapy options [16], underscoring the need for novel drug candidates.

In this study, we investigate the therapeutic potential of HQ-loaded polymeric NPs made of poly(*L*-lactide-*co*-glycolide), PLGA, against breast cancer. PLGA is among the most commonly studied polymers in drug delivery applications due to its excellent biocompatibility, tuneable degradation and release characteristics, and long clinical history [17]. The high versatility of PLGA allows for the generation of particles in different sizes [18], using various preparation techniques [19], also in large production scales [20,21]. We report on the preparation of HQ-loaded PLGA NPs (HQ-NP) and evaluate their effects on breast cancer cell lines MCF-7 and MDA-MB-231 in comparison to soluble HQ (HQ_{sol}). Our findings indicate that HQ-NPs could generate more potent and selective toxicity against both cell types via inducing mitochondrial dysfunction and oxidative stress, which is likely to be driven by the putative inhibition of voltage-gated ion channels as suggested by molecular docking studies. The obtained results suggest that repositioning of HQ as nanoformulations against breast cancer could potentially advance the development of more effective therapies, which should be validated in future *in vivo* studies.

2. Materials and methods

2.1. Materials

Hydroquinidine (HQ), Resomer® 502 H poly(lactide-co-glycolide) (PLGA) (50:50 lactide:glycolide ratio, Mw 7000–17000), poly(vinyl alcohol) (PVA) (Mw 9000), dichloromethane (DCM), Dulbecco's Modified Eagle's Medium (DMEM), fetal bovine serum (FBS), and dimethyl sulfoxide (DMSO) were purchased from Sigma-Aldrich. Alexa Fluor®488 Annexin V/Dead Cell Apoptosis Kit, Total ROS Assay Kit, and Click-iT™ EdU (5-Ethynyl-2-deoxyuridine) Cell Proliferation Kit were obtained from Thermo Fisher Scientific. All chemicals were used as received.

2.2. Preparation and characterization of nanoparticles

2.2.1. Particle preparation

Empty and HQ-loaded PLGA NPs were prepared using an emulsion and solvent evaporation–extraction method as described previously [22]. Briefly, 10 mg of PLGA in 0.6 mL of DMSO: DCM mixture (1:5 ratio) was added to 2.5 mL of aqueous phase containing 2 % PVA solution and sonicated for 2 min at 40 % amplitude using a Branson S250 probe sonicator. The organic phase was evaporated overnight, and NPs were collected by centrifugation at 21 300 *g* for 35 min, washed three times with ultrapure water, and lyophilized. HQ-loaded NPs were prepared using the same method with an addition of 1 mg, 2 mg, or 4 mg HQ into the organic phase.

2.2.2. Particle characterization

The size and polydispersity index (PDI) of PLGA NPs were analyzed by dynamic light scattering using a Zetasizer Nano-ZS (Malvern Instruments). The morphology of the nanoparticles was characterized using a multi-mode NanoScope atomic force microscope (AFM) (Bruker). 100 μL of 1 mg/mL particle suspension was dried on clean glass substrates and particles were imaged in tapping mode. Silicon nitride cantilevers with nominal spring constants of 0.4 N/m (Bruker) were used for the imaging. The scan rate was set at 1 Hz. 256 lines with 256 points per line were recorded during image acquisition. AFM images were analyzed using NanoScope analysis software v3.0 (Bruker). The HQ content of the particles was quantified using UV–Vis spectroscopy. A 10 mg/mL HQ-NP suspension was prepared in a 1:10 DMSO: water mixture, and then the absorbance at 330 nm was recorded using a Cary 60 UV–vis spectrophotometer (Agilent Technologies). Blank measurements were done using empty PLGA nanoparticles at the same concentration as the HQ-NPs for baseline correction to eliminate any influence of scattering or background interference in the absorbance readings at 330 nm. A standard series of HQ in 1:10 DMSO: water mixture (10–200 μg/mL) was prepared, and the absorbance values at 330 nm were used to plot a calibration curve. The equation of the linear fit of the curve was used to calculate the amount of HQ in the particles. Then, the encapsulation efficiency (EE) and drug loading (DL) were calculated using Equations (1) and (2), respectively.

$$\text{Encapsulation Efficiency } (\%) = \frac{\textit{amount of drug in NPs}}{\textit{total amount of drug used to prepare NPs}} \times 100 \quad \text{(Eq. 1)}$$

$$\text{Drug Loading } (\%) = \frac{\textit{amount of drug in NPs}}{\textit{total weight of NPs}} \times 100 \quad \text{(Eq. 2)}$$

2.3. Cell culture and chemicals

Human breast cancer cell lines MCF-7 (ATCC Number: HTB-22) and MDA-MB-231 (ATCC Number: HTB-26), and human embryonic kidney cells (HEK293, ATCC Number: CRL-1573) were cultured in DMEM supplemented with 10 % FBS and 1 % penicillin/streptomycin. Cultures were maintained at 37 °C in a humidified incubator with 5 % CO2. Cells were passaged upon reaching 80 % confluence, with growth monitored using an inverted microscope. HQ was dissolved in DMSO to create stock solutions, which were then diluted in complete culture medium to the desired concentrations for subsequent experiments.

2.4. Cell viability assay

MTT assay was used to study cell viability. MCF-7 and MDA-MB-231 cells were seeded in 96-well plates at densities of 0.1×10^5 and 0.05×10^5 cells per well for 24- and 48-h treatments, respectively. HEK293 cells were tested in parallel as 'healthy' controls to investigate the selectivity of HQ against breast cancer cell lines. After attachment, cells were exposed to various concentrations of HQ-loaded PLGA NPs (0.0001 mM–0.4 mM) for the specified durations. Controls included culture medium alone (negative) and 10 % DMSO in culture medium (positive). Following the manufacturer's protocol, absorbance was measured at 570 nm. IC_{50} values were calculated using dose-response curve fitting with the "drc" package in R. The selectivity index (SI) of soluble HQ and HQ-NPs were determined by dividing the IC_{50} values of the healthy cell line HEK293 by those obtained for MCF7 and MDA-MB-231 cells.

2.5. Colony formation assay

To study the long-term effects of HQ-NPs on colony formation, 2×10^3 cells per well were seeded in 96-well plates. Medium was replaced every two days until cells reached at least 80 % confluence. Cells were then fixed with methanol, stained with Crystal Violet, and imaged using a bright-field microscope. Colony number and intensity were quantified using the ColonyArea plugin of ImageJ software.

2.6. Scratch-wound assay

Cell migration was assessed using an *in vitro* scratch-wound assay. Cells were seeded in 24-well plates and grown to confluence. After creating a cell-free zone with a pipette tip, cells were treated with HQ-loaded PLGA NPs at the 48-h IC_{50} concentration. Wound closure was monitored at 0 and 24 h post-wounding using bright-field microscopy. Wound areas were calculated using the MRI_Wound_Healing_Tool plugin in ImageJ.

2.7. Spheroid formation assay

To evaluate anchorage-independent growth, a soft agar colony formation assay was performed. A base layer of agar and culture medium was prepared in 12-well plates. Cells were then suspended in a mixture of agar solution and either control medium or HQ-NP containing medium at the 24-h IC_{50} concentration. After 30 days of incubation, colonies were imaged and analyzed using ImageJ with the ParticleSizer plugin.

2.8. Apoptosis assay

Apoptotic effects were analyzed using the Alexa Fluor®488 Annexin V/Dead Cell Apoptosis kit. Cells were seeded in 12-well plates and treated with HQ-NPs at the IC_{50} concentration for 24 h. Following treatment, cells were processed according to the manufacturer's instructions and analyzed by flow cytometry to determine the proportion of apoptotic and necrotic cells.

2.9. Reactive oxygen species (ROS) assay

ROS levels were determined using the Total ROS Assay Kit. MCF-7 and MDA-MB-231 cells were plated at a density of 5×10^5 cells per well in 6-well plates and incubated for 24 h. After this incubation period, 100 μL of 1 × ROS Assay Stain was added to the wells to label the cells, followed by a 60-min incubation at 37 °C in a 5 % CO_2 environment. The cells were then treated with the tested compounds for 28 h to promote ROS generation. ROS levels in live cells were subsequently analyzed using flow cytometry (BD Biosciences, San Jose, CA, USA).

2.10. Mitochondrial membrane potential (MMP) assessment

MCF-7 and MDA-MB-231 cells were seeded at a density of 5×10^5 cells per well in 6-well plates and incubated for 24 h. Following this, cells were either left untreated or exposed to tested compounds for an additional 48 h. After treatment, cells were collected and incubated with 400 nM TMRE for 30 min at 37 °C in a humidified incubator with 5 % CO_2. Subsequently, the cells were washed and resuspended in ice-cold PBS by centrifugation (2000 rpm, 3 min). Changes in MMP, indicative of early apoptotic events, were quantitatively analyzed using the TMRE-Mitochondrial Membrane Potential Assay Kit (Abcam, ab113852, Cambridge, UK), and the fluorescence was measured via flow cytometry (BD Biosciences, San Jose, CA, USA).

2.11. Cell proliferation assay

Cell proliferation was assessed using the Click-iT™ EdU (5-Ethynyl-2-deoxyuridine) Cell Proliferation Kit. Cells were seeded in 96-well plates, treated with HQ-NPs for 24 h, and then incubated with EdU. After fixation and permeabilization, EdU incorporation was detected following the kit's protocol. Nuclei were counterstained with Hoechst dye. Fluorescence microscopy images were analyzed using ImageJ to quantify EdU-positive and total cell numbers.

2.12. In silico analysis

Molecular docking studies were performed using Autodock Vina [23, 24] available in the SwissDock 2024 web tool. The affinity of HQ towards potassium channels Kv1.1 (PDB ID: 2AFL), Kv1.3 (PDB ID: 7EJ1), and Kv11.1 (PDB ID: 5VA1) and sodium channels Nav1.7 (PDB IDs: 6J8H, 5EK0, and 7W9K) was studied in comparison to known small molecule inhibitors of the corresponding channels (Table S.I. 1). The SMILES of the compounds were retrieved from the PubChem database (https://pubchem.ncbi.nlm.nih.gov/). The docking parameters were kept to their default values except for sampling exhaustivity, which was set as 64. The calculated binding energies were plotted using OriginPro software. Targeted docking studies were conducted on the active sites of Kv1.1 and NaV1.7 utilizing AutoDock Vina, integrated with PyRx. The grid coordinates were established at 69Å × 26Å × 17 Å for Kv1.1 and 210Å × 214Å × 208 Å for NaV1.7, with a precise grid spacing of 0.375 Å for docking accuracy. The docking configuration exhibiting the lowest binding affinity was chosen for further investigation. Visualization of the docking outcomes was performed using Pymol software and the Proteinsplus tool (https://proteins.plus/) to analyze the binding pose and chemical interactions. For further chemoinformatics analysis, potential targets for HQ were predicted using the Swiss target prediction tool [25]. A combination of 2D and 3D similarity assessments generated a list of predicted proteins, which were subsequently analyzed for Kyoto Encyclopedia of Genes and Genomes (KEGG) pathway enrichment using the 'ClusterProfiler' package [26] in the R environment. The top 20 KEGG pathways were plotted.

3. Results

3.1. Preparation and characterization of HQ-loaded PLGA NPs

Empty and HQ-loaded PLGA NPs (eNPs and HQ-NPs, respectively) were prepared via an emulsion-solvent extraction method using a probe sonicator (Fig. 1a). Fine emulsion droplets formed through high-frequency vibrations were stabilized by the surfactant (PVA), and the hardened NPs were obtained after evaporation and extraction of the organic phase. Different amounts of HQ were added to the organic phase to find the best formulation in terms of size distribution and drug loading. The process yielded monodisperse NPs of approx. 150 nm size and a small polydispersity index (PDI, <0.2) for both eNPs and HQ-NPs (Fig. 1b). The lyophilization step resulted in a remarkable increase in the size of eNPs and HQ-NPs prepared using 2 mg HQ accompanied by an increase in PDI (Fig. 1c). Lyophilization is typically carried out in the presence of cryoprotectants and is known to cause several stresses leading to physical instability of nanoparticles [27]. Although we did not use a cryoprotectant for the lyophilization step, the PVA surfactant used in the formulation has been shown to exhibit a cryoprotective effect itself [28]. The HQ-NPs prepared using 4 mg HQ displayed only a small increase in size upon lyophilization with a PDI <0.2, and exhibited a spherical morphology as determined using atomic force microscopy (Fig. 1d). Therefore, this formulation was selected for further analysis.

The encapsulated HQ was quantified as 52 μg/mg particle using UV–vis. absorption spectroscopy, which corresponded to 9.6 % encapsulation efficiency (EE) and 5.2 % drug loading (DL). The characteristics of eNPs and HQ-NPs used in the following *in vitro* studies are summarized in Table 1.

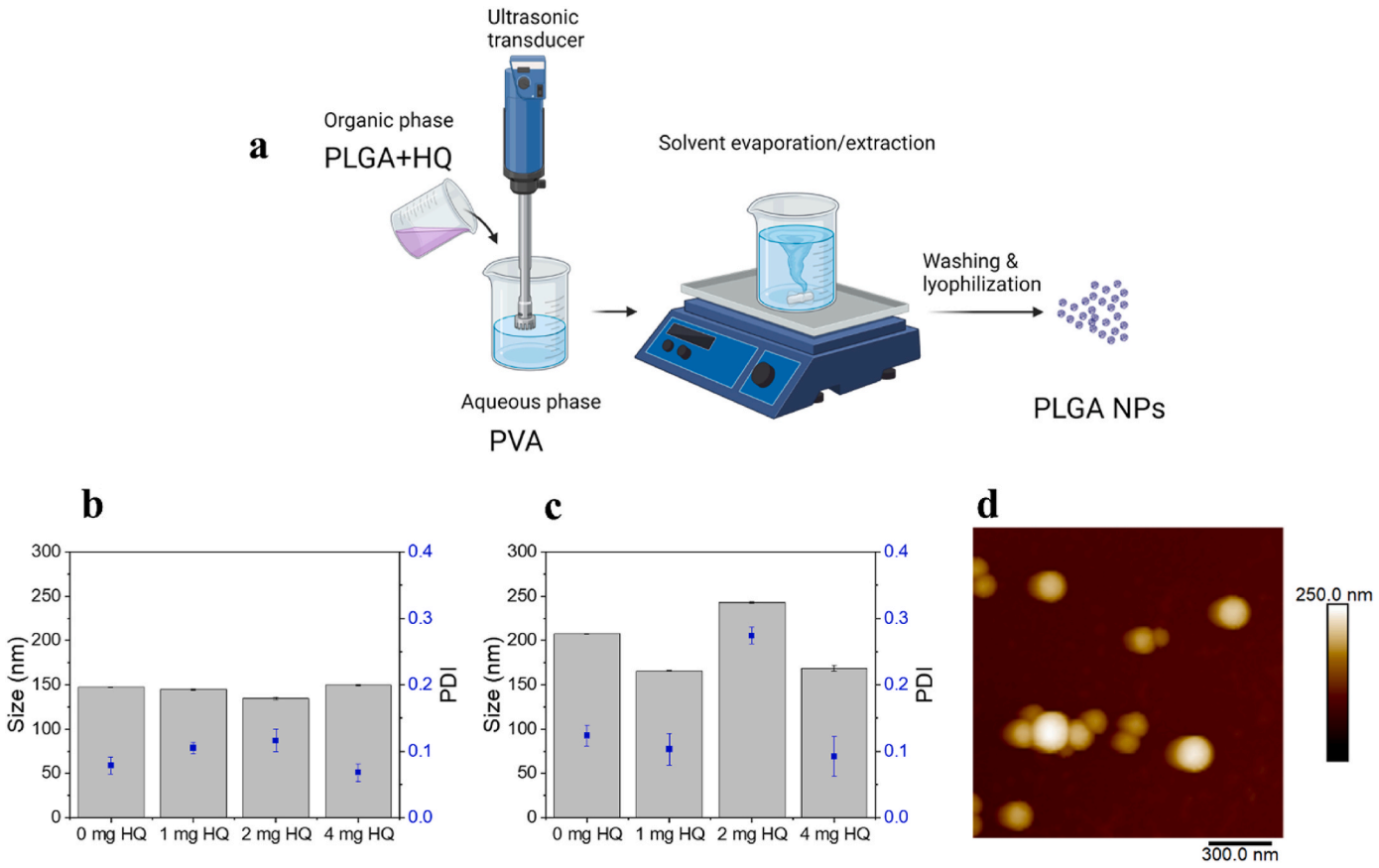

Fig. 1. (**a**) Schematic presentation of PLGA NP preparation process. Size and polydispersity index (PDI) of eNPs (0 mg HQ) and HQ-NPs obtained by dynamic light scattering before (**b**) and after (**c**) lyophilization. The amount of HQ used for the preparation of NPs is depicted as 'mg HQ'. (**d**) Atomic force microscopy height image of HQ-NPs. Scan size: 1.5 x 1.5 μm.

Table 1
Properties of eNPs and HQ-NPs used in the *in vitro* studies.

	Size (nm)	PDI[1]	EE (%)[2]	DL (%)[3]
eNP	207.6 (±0.4)	0.12 (±0.02)	n. a.	n. a.
HQ-NP	168.7 (±2.1)	0.09 (±0.03)	9.6	5.2

[1]PDI: polydispersity index, [2]EE: encapsulation efficiency, [2]DL: drug loading, n. a.: not applicable.

3.2. Nanoencapsulation improves potency and selective toxicity of HQ against breast cancer cell lines

The IC_{50} values of HQ_{sol} and HQ-NPs were determined on MCF7 and MDA-MB-231 breast cancer cell lines using an MTT cytotoxicity assay, which showed a clear dose-dependent toxicity for both cell types. The MTT assays revealed that HQ-NPs exhibited a significant toxicity against both MCF7 (Fig. 2a) and MDA-MB-231 (Fig. 2b) breast cancer cells, with an IC_{50} of 33 μM and 27 μM, respectively. In contrast, empty nanoparticles (eNP) tested in equal amounts as HQ-loaded counterpars showed no toxicity at the highest concentration tested. This stark difference indicates that the nanoparticle delivery system itself is non-toxic to the cells. In comparison to HQ-NPs, the IC_{50} value of free drug (HQ_{sol}) was approximately 10-fold and 8-fold higher for MCF7 (320 μM) and MDA-MB-231 (210 μM) cell lines, respectively (Table 2). This improved potency clearly highlighted the advantages of the nanoparticle-based delivery of HQ.

HEK293 were also tested in parallel as 'healthy' counterparts to study whether HQ toxicity was selective towards the breast cancer cell lines (Figure S.I.1). The selectivity index (SI) values derived from MTT assays by dividing the IC_{50} values for the HEK293 cells by the IC_{50} values for the breast cancer cell lines revealed distinct profiles for the tested compounds (Table 2). Usually, a treshold of 3 is set for SI values to indicate the desired selectivity against cancer cells [29]. The free drug HQ_{sol} exhibited moderate selectivity toward MDA-MB-231 cells (SI = 3.02) but limited selectivity for MCF-7 cells (SI = 1.98), whereas its nanoencapsulated counterpart, HQ-NP, demonstrated significantly enhanced selectivity for both breast cancer cell lines, with SI values of 5.37 (MCF-7) and 6.56 (MDA-MB-231). Nanoencapsulation improved SI values by more than two-fold compared to HQ_{sol}, highlighting the role of nanoparticle delivery in enhancing therapeutic specificity. Among the standard drugs, Doxorubicin showed higher selectivity for MCF-7 (SI = 7.4) than MDA-MB-231 (SI = 4.66), while Paclitaxel exhibited strong selectivity for MCF-7 (SI = 13.3) and moderate selectivity for MDA-MB-231 (SI = 5.7). Notably, HQ-NP's SI values approached those of Doxorubicin and Paclitaxel, particularly in MDA-MB-231 cells (6.56 vs. 4.66 and 5.7, respectively), despite its higher IC_{50} values.

3.3. HQ-NPs inhibit growth and migration of MCF7 and MDA-MB-231 cells

To further investigate the anti-carcinogenic properties of HQ-NP, we performed scratch-wound assay and compared four experimental groups: Control (no treatment), HQ-NP (in IC_{50} concentrations), HQ_{sol} (in the same concentration as encapsulated HQ), and eNP (equivalent nanoparticle concentration as HQ-NP, without drug) (Fig. 3). Significant differences in cell migration among these groups were observed for both MCF7 (Fig. 3a) and MDA-MB-231 cells (Fig. 3b). Control MCF7 cells efficiently closed the wound, with only a 12 % relative gap remaining after 24 h (Fig. 3a). HQ-NP treatment, however, dramatically inhibited

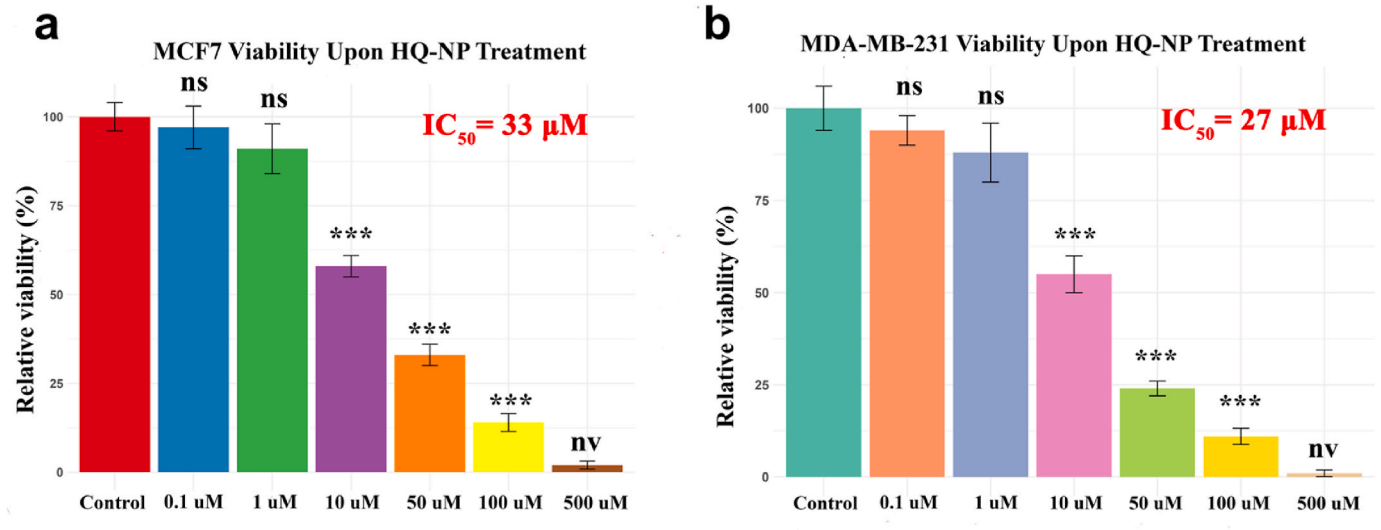

Fig. 2. The comparative viability of MCF7 (**a**) and MDA-MB-231 (**b**) cells treated with different concentrations of HQ-NP for 24 h, highlighting its dose-dependent anti-carcinogenic effects on cell viability. Statistical significance is represented as ***$p < 0.001$. ns; non-significant, nv; non-viable.

Table 2
IC_{50} values and selectivity index (SI) of HQ_{Sol},HQ-NP, Doxorubicin, and Paclitaxel.

	$IC_{50} \pm SE$ (µM)			Selectivity Index (SI)	
Compound	MCF-7	MDA-MB-231	HEK-293	MCF-7	MDA-MB-231
HQ_{Sol}	320 ± 17.4	210 ± 11.6	633 ± 70.2	1.98	3.02
HQ-NP	33 ± 2.8	27 ± 3.4	177 ± 12.4	5.37	6.56
Doxorubicin	0.5 ± 0.08	0.8 ± 0.11	3.7 ± 0.4	7.4	4.6
Paclitaxel	0.015 ± 0.001	0.035 ± 0.0014	0.2 ± 0.009	13.3	5.7

cell migration, leaving an 86 % relative gap ($p < 0.001$ compared to control). eNP-treated cells behaved similarly to the control group, with a 16 % relative gap ($p > 0.05$), while HQ_{sol} showed intermediate effectiveness, resulting in a 25 % relative gap ($p < 0.01$). These results significantly differed across all groups, highlighting the superior anti-migratory effect of HQ-NP.

The wound healing assay with MDA-MB-231 cells corroborated our findings in MCF7 cells, demonstrating the superior anti-migratory effects of HQ-NP (Fig. 3b). Control MDA-MB-231 cells exhibited robust migration, with only an 11 % relative gap after 24 h eNP-treated cells showed similar behavior, with a 10 % relative gap, again confirming the non-inhibitory nature of the nanoparticle system itself. HQ_{sol} demonstrated moderate inhibition of migration, resulting in a 23 % relative gap. However, HQ-NP treatment profoundly impaired cell migration, leaving an 83 % relative gap.

We then examined the impact of these treatments on both anchorage-dependent and independent growth using colony formation (CFA) and soft agar (SFA) assays, respectively (Fig. 4). In both 2D (Fig. 4a) and 3D (Fig. 4b) culture conditions, HQ-NP demonstrated remarkable potency in inhibiting MCF7 cell growth compared to all other groups ($p < 0.001$). eNP-treated cells showed growth patterns similar to the control group ($p > 0.05$), further confirming the non-toxic nature of the nanoparticle system. HQ_{Sol}, at the tested concentration, exhibited only mild growth-limiting effects on MCF7 cells in both assays, and there was a significant difference in growth capacity between HQ_{Sol} and HQ-NP treated MCF7 cells ($p < 0.001$).

Examination of anchorage-dependent and independent growth of MDA-MB-231 cells through colony formation and soft agar assays yielded results highly consistent with those observed for MCF7 cells. HQ-NP exhibited superior inhibition of MDA-MB-231 cell growth in both 2D (Fig. 4c) and 3D (Fig. 4d) culture conditions compared to all other treatment groups ($p < 0.001$). eNP-treated cells displayed growth patterns similar to the control group ($p > 0.05$), while HQ_{Sol} showed moderate growth-limiting effects with significant growth-limiting activity in comparison to the control group ($p < 0.001$).

Collectively, these results provide compelling evidence that HQ-NP significantly outperforms HQ_{Sol} in inhibiting migration and both 2D and 3D growth of MCF7 and MDA-MB-231 breast cancer cells.

3.4. HQ-NP induces apoptosis, mitochondrial dysfunction, and suppresses proliferation in MCF7 cells

Following our initial findings, we conducted in-depth cellular analyses on MCF7 and MDA-MB-231 cells to elucidate the mechanisms underlying the observed anti-cancer effects. Given the lack of significant differences between eNP and control groups in growth and migration assays, we focused on control, HQ_{Sol}, and HQ-NP groups in the subsequent experiments.

Apoptosis assays revealed a marked increase in programmed cell death following HQ-NP treatment (Fig. 5a, Figure S.I.2). Flow cytometry analysis of Annexin V/7AAD staining in MCF7 cells showed that the apoptosis rate increased from 6 % in the control group to 16.9 % with HQ_{Sol} treatment, and further to 25.2 % with HQ-NP treatment. This represents a significant 3.7-fold increase in apoptotic cells for the HQ-NP treated group compared to the control ($p < 0.01$). There was no significant difference in apoptosis rate between HQ_{Sol} treatment and control groups ($p > 0.05$). Notably, the significant difference ($p < 0.01$) in apoptosis rates between HQ_{Sol} and HQ-NP groups underscores the enhanced pro-apoptotic effect of HQ when delivered via nanoparticles.

To further investigate the mechanism of apoptosis induction, we analyzed mitochondrial membrane potential (MMP, Fig. 5b). Flow cytometry data revealed a significant shift in the number of cells exhibiting altered mitochondrial function. The proportion of cells with lower MMP increased from 12.2 % in the control group to 22.8 % in

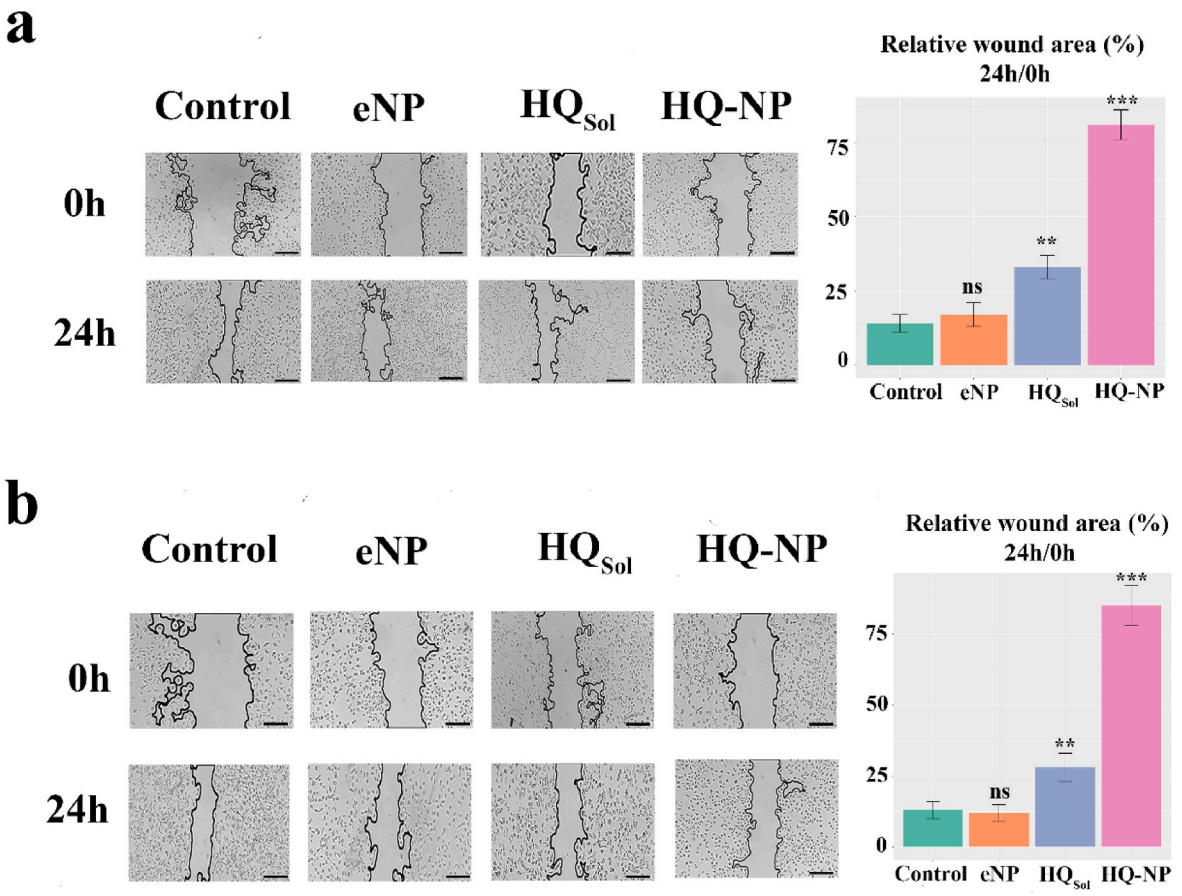

Fig. 3. Scratch-wound assay shows that HQ-NP substantially, HQ_{Sol} mildly inhibits cell migration and wound closure within 24 h for MCF7 (**a**) and MDA-MB-231 (**b**) cells. h; hours, eNP; empty nanoparticle, HQ_{Sol}; Soluble hydroquinidine, HQ-NP; Hydroquinidine-loaded PLGA nanoparticles. **p < 0.01, ***p < 0.001, ns; non-significant (treatment groups vs control). Scale bars: 100 μm.

HQ_{Sol}-treated cells, and further to 29.5 % in HQ-NP-treated cells. This progressive increase in cells with compromised MMP aligns with the observed rise in apoptosis rates, indicating that HQ-NP treatment significantly impacts mitochondrial integrity ($p < 0.01$). Interestingly, HQ_{Sol} treatment considerably increased the mitochondrial dysfunction compared to the control group ($p < 0.01$). As with the apoptosis assay, the significant difference between HQ_{Sol} and HQ-NP groups ($p < 0.01$) in MMP disruption further demonstrates the increased efficacy of nano-formulated HQ.

Consistent with these findings, we observed a marked elevation in reactive oxygen species (ROS) production in MCF7 cells treated with HQ-NP (Fig. 5c). Flow cytometry analysis showed that ROS levels were approximately 1.1 and 1.8 times higher in HQ_{Sol} and HQ-NP-treated cells, respectively, compared to non-treated controls. This significant increase ($p < 0.01$) in ROS production suggests that HQ-NP induces substantial oxidative stress, likely contributing to its potent anti-carcinogenic effects.

To further elucidate the mechanisms underlying the observed anti-cancer effects, we complemented our apoptosis and ROS analyses with an assessment of cell proliferation using EdU labeling (Fig. 5d). This assay provided crucial insights into the impact of HQ-NP on cell cycle progression and division.

In MCF7 cells, we observed a marked decrease in the number of proliferating cells following both HQ_{Sol} and HQ-NP treatments ($p < 0.001$), with HQ-NP demonstrating superior anti-proliferative effects. The ratio of EdU-positive cells to the total cell population was 45 % in the control group, indicating a robust baseline proliferation rate. This ratio decreased significantly to 28 % in HQ_{Sol}-treated cells, demonstrating the anti-proliferative effect of hydroquinidine alone. However, the most striking result was observed in the HQ-NP-treated group, where the proportion of proliferating cells diminished to 12 %. This represents a remarkable 3.75-fold decrease in proliferation rate compared to the control group. The significant difference between HQ_{Sol} and HQ-NP-treated groups ($p < 0.01$) in terms of inhibition of proliferation is particularly noteworthy, which aligns well with our previous observations on inducing apoptosis and ROS generation, further emphasizing the enhanced activity of HQ when delivered as nanoformulations.

3.5. HQ-NP elicits consistent multi-modal anti-cancer effects in MDA-MB-231 cells

Parallel studies conducted on MDA-MB-231 cells corroborated our findings in MCF7 cells, further emphasizing the broad applicability of HQ-NP across different breast cancer subtypes. Flow cytometry analysis of Annexin V/7AAD staining revealed a substantial increase in apoptosis rates in MDA-MB-231 cells following HQ-NP treatment (Fig. 6a, Figure S.I.3). The percentage of apoptotic cells rose from 7.0 % in the control group to 12.0 % with HQ_{Sol} treatment, and markedly increased to 17.5 % in the HQ-NP treated group. This represents a significant 2.5-fold increase in apoptotic cells for the HQ-NP treated group compared to the control ($p < 0.001$). The notable difference ($p < 0.01$) between HQ_{Sol} and HQ-NP groups further underscores the enhanced pro-apoptotic effect of nanoparticle-delivered HQ in this triple-negative breast cancer cell line.

MMP analysis in MDA-MB-231 cells aligned with the apoptosis data, showing a progressive increase in mitochondrial dysfunction across treatment groups (Fig. 6b). The proportion of cells with compromised MMP increased from 12.0 % in the control group to 16.7 % in HQ_{Sol}-

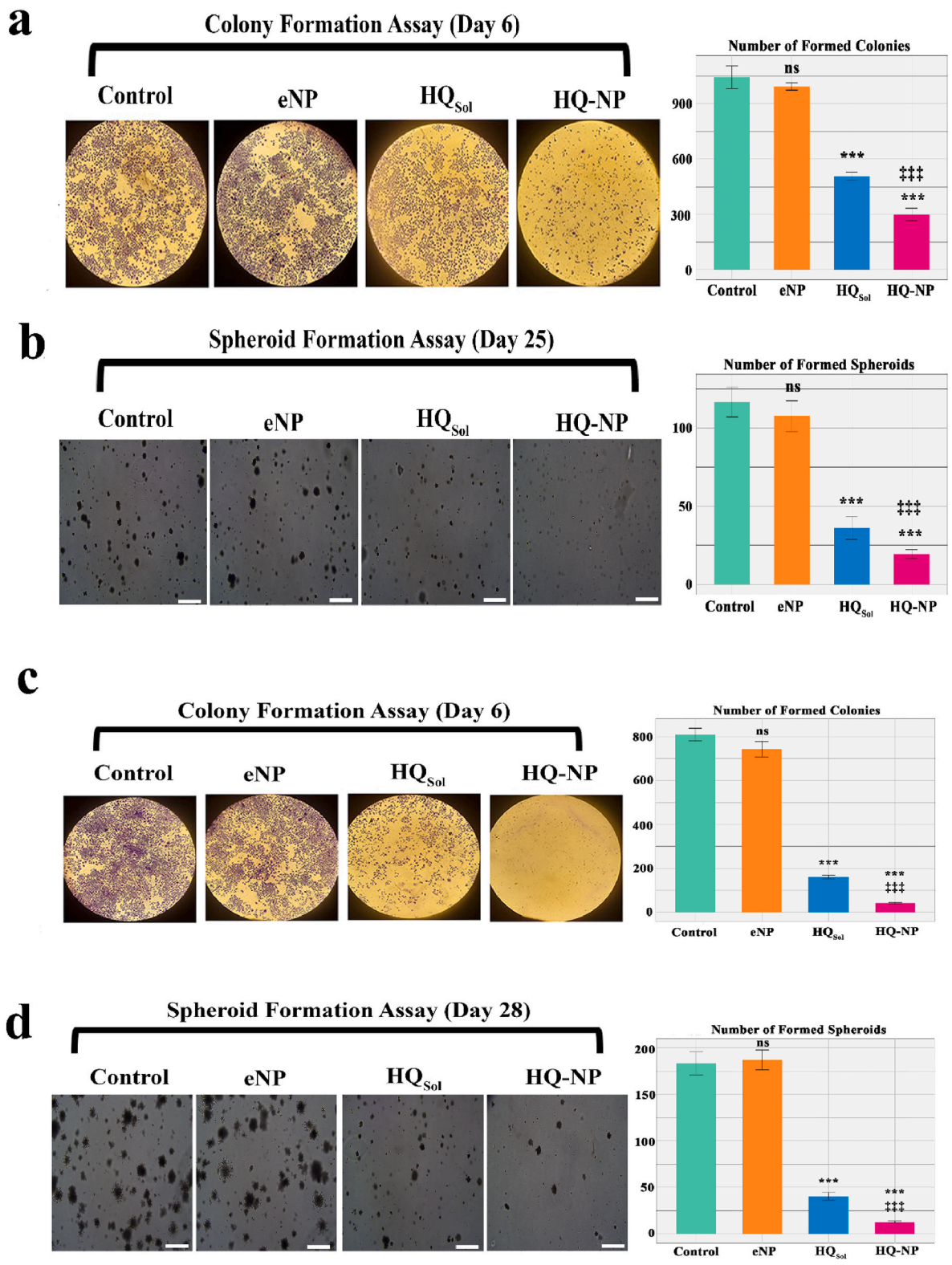

Fig. 4. Colony formation and spheroid formation assays for MCF7 (**a** and **b**, respectively) and MDA-MB-231 (**c** and **d**, respectively) cells after treatment with eNP, HQ_{Sol}, and HQ-NP showing diverse effects on colony formation capability and three-dimensional growth of spheroids. eNP; empty nanoparticle, HQ_{Sol}; Soluble hydroquinidine, HQ-NP; Hydroquinidine-loaded PLGA nanoparticles. ***$p < 0.001$. ns; non-significant (treatment groups vs control). ‡‡‡$p < 0.001$ (HQ-NP vs HQ_{Sol}). Scale bars: 100 μm.

treated cells, and further to 28.4 % in HQ-NP-treated cells. This substantial shift in MMP disruption correlates strongly with the observed increase in apoptosis rates, indicating that HQ-NP treatment significantly impacts mitochondrial integrity in MDA-MB-231 cells ($p < 0.001$).

MDA-MB-231 cells displayed lower basal levels of ROS in comparison to MCF 7, which was markedly elevated upon treatment with HQ-NP (Fig. 6c). Flow cytometry analysis demonstrated that ROS levels were

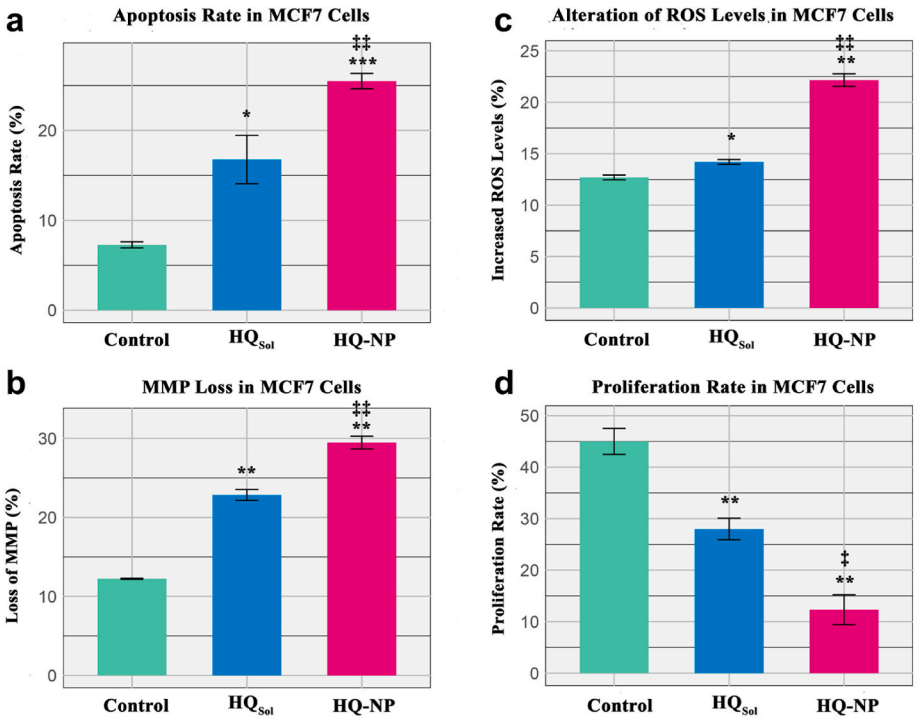

Fig. 5. (**a**) Flow cytometry analysis of apoptosis rates in MCF7 cells using Annexin V/7AAD staining, comparing control and treatment groups to show HQ-NP's pro-apoptotic effect. (**b**) MMP staining and flow cytometry analysis of MCF7 cells, illustrating HQ-NP's impact on mitochondrial health and function. (**c**) Flow cytometry measurement of ROS levels in MCF7 cells, comparing control and HQ-treated cells to highlight oxidative stress induced by HQ_{Sol} and HQ-NP. (**d**) Cell divison rate comparison among groups providing insights into cellular proliferation dynamics. Statistical comparisons between treatment groups and the control group are marked by asterisks (*p < 0.05, **p < 0.01). Differences between HQ_{Sol} and HQ-NP groups are represented by the ‡ symbol (‡p < 0.05, ‡‡p < 0.01).

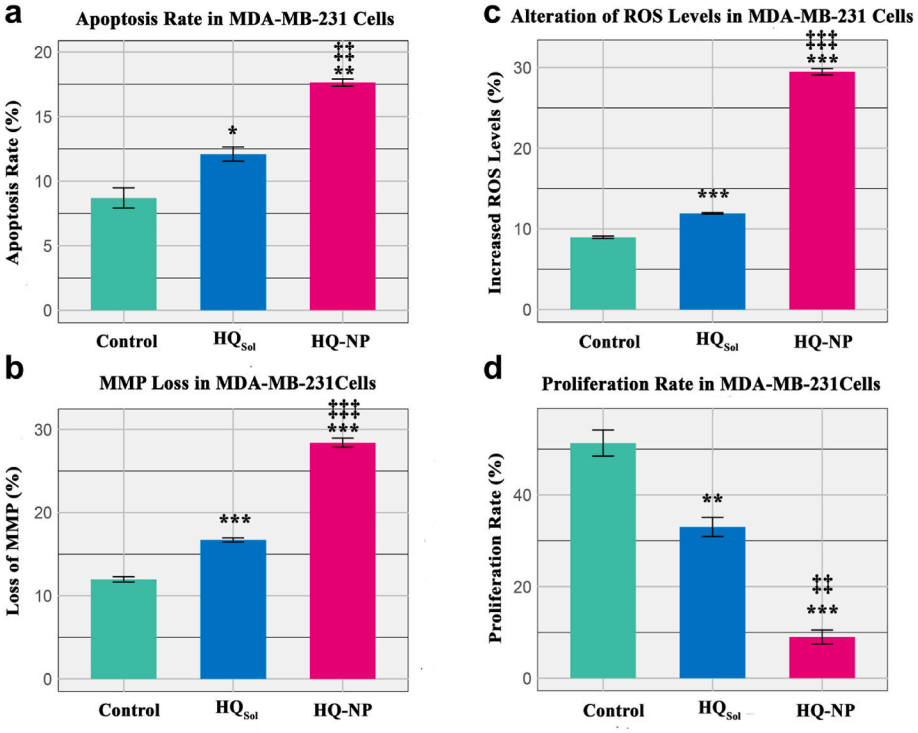

Fig. 6. (**a**) Evaluation of apoptosis rates in MDA-MB-231 cells with Annexin V/7AAD staining by comparing control and treatment groups. (**b**) Mitochondrial integrity upon treatment was assessed using MMP assay and flow cytometry analysis to demonstrate HQ's impact on mitochondrial function. (**c**) Measurement of ROS levels in MDA-MB-231 cells by flow cytometry, comparing control and HQ-treated groups to highlight HQ-induced oxidative stress. **(d)** Measurement of EdU-labeled proliferating cells. Statistical significance between treatment groups and the control group is indicated by asterisks: *p < 0.05, **p < 0.01, and ***p < 0.001. ‡ symbol denotes statistical significance between HQ_{Sol} and HQ-NP groups. ‡‡p < 0.01, ‡‡‡p < 0.001.

approximately 1.3 and 3.3 times higher in HQ_{Sol} and HQ-NP-treated cells, respectively, compared to control cells. This significant increase ($p < 0.001$) in ROS production suggests that HQ-NP induces substantial oxidative stress in MDA-MB-231 cells, likely contributing to its potent anti-carcinogenic effects in this aggressive breast cancer subtype.

In MDA-MB-231 cells, we observed a substantial decrease in the proliferating cell population following both HQ_{Sol} and HQ-NP treatments, with HQ-NP again demonstrating prominent anti-proliferative effects (Fig. 6d). The control group exhibited a baseline proliferation rate of 52 %, as indicated by the ratio of EdU-positive cells to the total cell population. This ratio decreased markedly to 33 % in HQ_{Sol}-treated cells, showcasing the inherent anti-proliferative effect of hydroquinidine. However, the most pronounced effect was seen in the HQ-NP-treated group, where the proportion of proliferating cells dropped dramatically to only 9 %. This represents a striking 5.8-fold decrease in proliferation rate compared to the control group and a significant reduction even when compared to the HQ_{Sol}-treated cells ($p < 0.001$).

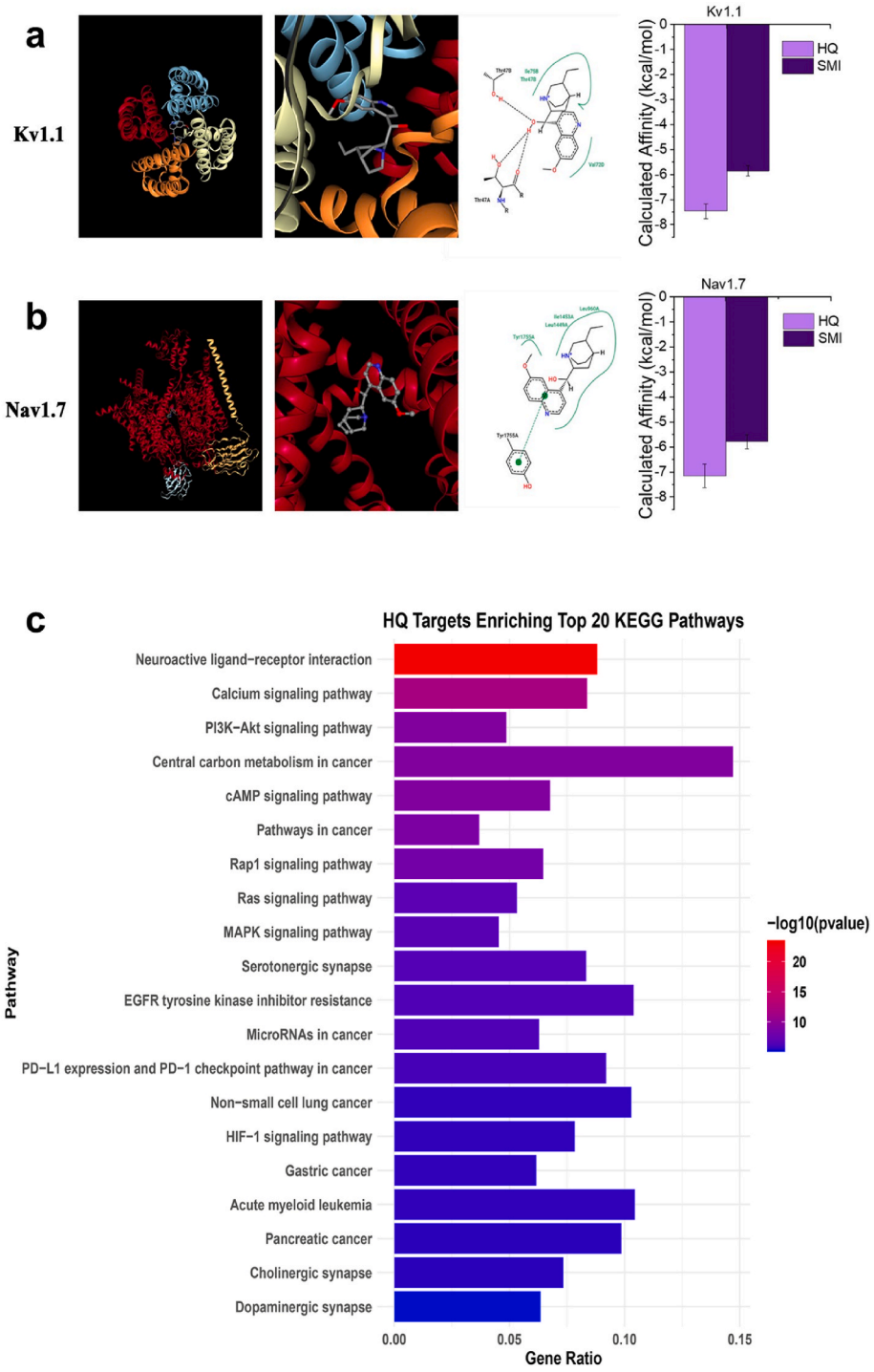

Fig. 7. 2D and 3D visualization of interactions and calculated free energies of binding of HQ in comparison to known small molecule inhibitors (SMI) for **(a)** Kv1.1 and **(b)** Nav1.7. **(c)** Functional annotation of predicted HQ target proteins.

3.6. HQ displays a high affinity towards Kv1.1 and Nav1.7

In the present study, we also conducted a comprehensive investigation of the potential interactions between the HQ and two key proteins implicated in cancer progression-the voltage-gated potassium and sodium channels. Molecular docking analysis revealed the putative binding pose of HQ within the Kv1.1 and Nav1.7 protein structures (Fig. 7). The docking results suggest that HQ may interact with amino acid residues lining the binding pocket of target proteins and potentially modulate the channels' activity. The free energies of binding of HQ to Kv1.1, Kv1.3, Kv11.1 and Nav1.7 in comparison to their known small molecule inhibitors (SMI) revealed high affinity of HQ towards these channels (Figure S.I.4). Amitriptyline, a known inhibitor of Kv1.1 [30], displayed −5.85 (±0.20) kcal/mol of free energy of binding in molecular docking studies, while this value was calculated as −7.46 (±0.29) kcal/mol for HQ (Fig. 7a). Similarly, the free energies of binding to Nav1.7 were calculated as −7.16 (±0.47) kcal/mol and −5.78 (±0.29) kcal/mol, respectively, for HQ and Carbamazepine that is known as a sodium channel blocker (Fig. 7b) [31]. These ion channels have been reported to play key roles in regulating cellular excitability and physiology, and their dysregulation has been linked to altered cancer cell proliferation and migration [32–35].

Another compelling aspect of our findings is the enrichment of various cancer-related KEGG pathways by the predicted target proteins of HQ, as shown in Fig. 7c. The significant enrichment of cancer-related pathways, such as the PI3K-Akt and cAMP signaling, and central carbon metabolism, suggests the potential mechanisms for the observed potent anti-cancer properties of HQ. Beyond these pathways, our analysis also revealed perturbations in calcium signaling, MAPK pathway, microRNAs in cancer, non-small cell lung cancer, and gastric cancer pathways.

4. Discussion

Repurposing drugs for new therapeutic targets can strongly benefit from nanoencapsulation, which provides a versatile tool to steer the solubility, biodistribution, efficacy, and safety profiles of drugs towards their novel targets. We have previously demonstrated the anti-cancer efficacy of HQ, a class IA antiarrhythmic drug, across various cancer types, including lung, colon, pancreatic, hepatic, breast, and ovarian cancers [8–10]. Our current investigation focuses on repurposing HQ towards breast cancer cells via taking advantage of nanoencapsulation within PLGA nanoparticles. Comparative analyses with soluble drug (HQ_{sol}) have demonstrated that nanoencapsulation improved both potency and selectivity of HQ in both estrogen receptor-positive MCF7 and triple-negative MDA-MB-231 breast cancer cell lines. A key finding of our study is the significantly lower IC_{50} values of HQ-NP compared to HQ_{sol}, approximately 10 times lower in MCF7 cells and 8 times lower in MDA-MB-231 cells. These findings underscore the potential of HQ-NP as a selective therapeutic agent for breast cancer. Although the IC_{50} values of Doxorubicin and Paclitaxel were significantly lower (indicating greater potency), HQ-NP's SI values were comparable or even superior in MDA-MB-231 cells, suggesting a favorable balance between efficacy and selectivity. The improved selectivity of HQ-NP over HQ_{sol} likely stems from enhanced bioavailability, a hallmark of nanoparticle-mediated drug formulations. The ability to achieve therapeutic effects at substantially lower doses is particularly important in the context of reducing potential toxicity to healthy cells [36]. By encapsulating hydroquinidine in PLGA nanoparticles, we have effectively enhanced its bioavailability and cellular uptake, allowing for a more efficient delivery to cancer cells. This approach not only improves the therapeutic index of hydroquinidine but also aligns with the broader goal of developing more selective and less toxic cancer treatments.

We investigated the effects and possible action mechanisms of HQ-NPs on breast cancer cells. The observed growth-limiting, anti-migratory, pro-apoptotic, and anti-proliferative impacts of HQ-NP are in line with previous reports on hydroquinidine and structurally similar compounds such as quinine, hydroquinine, and quinidine [37–40]. These findings suggest a conserved mechanism of action among this class of molecules, potentially related to their interactions with cellular targets, particularly ion channels. Targeting ion channels, especially potassium channels, has emerged as a promising strategy to eradicate tumors [41]. Potassium channels play crucial roles in regulating cell proliferation, migration, and apoptosis, which are often dysregulated in cancer [42]. The overexpression of certain potassium channels in various cancer types, including breast cancer, provides a rationale for their targeting in cancer therapy [43]. For instance, Kv1.1 and Kv1.3 have been reported to sensitize tumor cells of different origins to cytotoxic drugs [44]. The study found a higher expression of Kv1.1 in MDA-MB-231 cells that are characterized with a higher metastatic ability in comparison to MCF-7 cells.

HQ exerts its anticancer effects primarily through the modulation of multiple ion channels. It has been shown to inhibit the IKr current by targeting HERG1 channels, leading to the prolongation of the action potential duration [45,46]. HERG1 expression is elevated in various cancers, including breast cancer, and its inhibition has been associated with reduced tumor aggressiveness [47–49]. Additionally, HQ inhibits the Nav1.5 channel, which is highly expressed in metastatic breast cancer cells and contributes to tumor progression by promoting proton efflux, epithelial-to-mesenchymal transition (EMT), and enhanced invasiveness [50,51]. *In silico* docking studies further suggested Kv1.1 and Nav1.7 as potential additional targets of HQ. Kv1.1 has been implicated in cancer biology, and Nav1.7 inhibition has been shown to suppress metastasis in several cancer types [52]. Disrupting the delicate ion balance required for cancer cell survival and proliferation upon HQ treatment might lead to cell cycle arrest and apoptosis. The enhanced efficacy of HQ-NP observed in our study could be attributed to improved delivery of hydroquinidine to these cellular targets, allowing for more efficient and prolonged modulation of potassium channel activity.

Our *in silico* analyses indicating the cancer-related pathways as potential targets of HQ are well-aligned with the observed potency of HQ against breast cancer. The identified pathways are known to be critical for the survival, proliferation, and metabolic reprogramming of cancer cells, and have been implicated in the regulation of ion channels [53,54]. The prominence of calcium signaling aligns with HQ's role as a multi-ion channel modulator, suggesting its anti-cancer effects may stem, in part, from disrupting intracellular ion balance—a mechanism critical for cancer cell survival and metastasis. Similarly, the MAPK pathway, which governs proliferation and apoptosis [55], underscores HQ's potential to inhibit oncogenic signaling cascades. Notably, the enrichment of disease-specific pathways (non-small cell lung cancer and gastric cancer) alongside broader cancer-associated pathways (microRNAs in cancer) implies a versatile inhibitory activity against diverse malignancies, potentially mediated by HQ's interference with transcriptional regulation and metabolic reprogramming. These pathways collectively highlight HQ's multi-targeted mechanism, disrupting key nodes in cancer cell survival, proliferation, and metabolic adaptation. Further experimental validation of these pathway interactions could clarify their contribution to HQ's observed potency and selectivity.

The consistent results observed across multiple assays, including cell viability, migration, colony formation, and molecular studies of apoptosis and proliferation, provide strong evidence for the multi-modal anticancer activity of HQ-NPs. The enhanced induction of apoptosis, increased ROS production, and significant suppression of cell proliferation suggest that HQ-NP targets multiple hallmarks of cancer simultaneously. This multi-faceted approach may contribute to its superior efficacy and potentially reduce the likelihood of drug resistance development, a common challenge in cancer therapy [56]. Furthermore, the comparable efficacy of HQ-NP in both MCF7 and MDA-MB-231 cells is particularly noteworthy. Triple-negative breast cancers, represented by MDA-MB-231 cells, are often more aggressive and have limited treatment options compared to hormone receptor-positive cancers. The potent effects of HQ-NP on MDA-MB-231 cells suggest its potential as a

valuable therapeutic option for this challenging breast cancer subtype.

While our findings are promising, it is important to acknowledge the limitations of this study. The current work is based on *in vitro* experiments, and animal studies are required to validate the efficacy and safety of HQ-NP *in vivo*. Such studies would provide crucial information on the pharmacokinetics, biodistribution, and potential off-target effects of HQ-NP in a physiological context. Additionally, while we have demonstrated the enhanced efficacy of HQ-NP in breast cancer models, it remains to be determined whether similar improvements are observed in other cancer types where hydroquinidine has shown promise. Expanding the investigation to include other cancer cell lines and *in vivo* models would provide a more comprehensive understanding of the broad applicability of HQ-NP as an anticancer agent.

5. Conclusions

Our study highlights the therapeutic promise of repurposing HQ for breast cancer treatment through nanoformulation. Encapsulating HQ within PLGA nanoparticles significantly enhanced its potency and selectivity against both estrogen receptor-positive and triple-negative breast cancer cell lines, as evidenced by marked reductions in IC_{50} values and improved selectivity indices relative to the soluble form. These enhancements are largely attributed to improved cellular uptake and bioavailability, which are among the key advantages of nanoparticle-based drug delivery systems.

Functional assays demonstrated that HQ-loaded nanoparticles effectively induce apoptosis, inhibit cell migration and proliferation, and elevate ROS levels, reflecting broad-spectrum antitumor activity. Complementary *in silico* pathway enrichment analyses identified calcium signalling, MAPK cascades, cancer-specific transcriptional regulation, and metabolic reprogramming as key pathways associated with HQ's multi-targeted effects. *In silico* analyses further revealed that HQ-NP can disrupt ionic homeostasis through modulation of key ion channels including HERG1, Kv1.1, and Nav1.5, which are known to contribute to tumor progression and metastasis.

While these *in vitro* results are promising, further *in vivo* studies are required to assess the pharmacokinetics, biodistribution, therapeutic index, and safety profile of HQ-NP. Overall, our findings support the development of HQ-NP as a novel nanotherapeutic that unites drug repurposing with nanoformulation, offering a potentially more effective and less toxic treatment strategy for breast cancer. This approach underscores the broader utility of integrating nanotechnology with repurposed drugs to overcome traditional pharmacokinetic barriers and enhance therapeutic precision.

CRediT authorship contribution statement

Turan Demircan: Writing – original draft, Visualization, Supervision, Funding acquisition, Formal analysis, Conceptualization. **Daela Milinkovic:** Investigation, Formal analysis, Data curation. **Esin Sakallı Çetin:** Writing – review & editing, Visualization, Formal analysis. **Ebrunur Aksu:** Investigation, Formal analysis, Data curation. **Oya Tagit:** Writing – original draft, Visualization, Supervision, Project administration, Formal analysis, Conceptualization.

Data availability statement

The data that supports the findings of this study are available in the supplementary material of this article.

Funding

The authors would like to thank EMBO for providing funding to facilitate the collaborative research visit that enabled this work (EMBO Scientific Exchange Grant number 10286).

Declaration of competing interest

The authors declare that they have no known competing financial interests or personal relationships that could have appeared to influence the work reported in this paper.

Appendix A. Supplementary data

Supplementary data to this article can be found online at https://doi.org/10.1016/j.jddst.2025.107098.

Data availability

Data will be made available on request.

References

[1] Y. Xia, M. Sun, H. Huang, W.-L. Jin, Drug repurposing for cancer therapy, Signal Transduct. Targeted Ther. 9 (1) (2024) 1–33, https://doi.org/10.1038/s41392-024-01808-1.
[2] S. Rayego-Mateos, R.R. Rodrigues-Diez, B. Fernandez-Fernandez, C. Mora-Fernández, V. Marchant, J. Donate-Correa, J.F. Navarro-González, A. Ortiz, M. Ruiz-Ortega, Targeting inflammation to treat diabetic kidney disease: the road to 2030, Kidney Int. 103 (2) (2023) 282–296, https://doi.org/10.1016/j.kint.2022.10.030.
[3] T. Czech, R. Lalani, M.O. Oyewumi, Delivery systems as vital tools in drug repurposing, AAPS PharmSciTech 20 (3) (2019) 116, https://doi.org/10.1208/s12249-019-1333-z.
[4] P.M. Giri, A. Banerjee, B. Layek, A recent review on cancer nanomedicine, Cancers 15 (8) (2023) 2256, https://doi.org/10.3390/cancers15082256.
[5] M. Najlah, Drug repurposing supported by nanotechnology: a promising strategy to fight cancer, Ther. Deliv. 12 (4) (2021) 267–269, https://doi.org/10.4155/tde-2021-0009, 12(4), 267–269.
[6] A. Mazzanti, R. Maragna, G. Vacanti, A. Kostopoulou, M. Marino, N. Monteforte, R. Bloise, K. Underwood, V. Tibollo, E. Pagan, C. Napolitano, R. Bellazzi, V. Bagnardi, S.G. Priori, Hydroquinidine prevents life-threatening arrhythmic events in patients with short QT syndrome, J. Am. Coll. Cardiol. 70 (24) (2017) 3010–3015, https://doi.org/10.1016/j.jacc.2017.10.025.
[7] L. Halperin, G. Mellor, M. Talajic, A. Krahn, R. Tadros, Z. Laksman, Quinidine effective for the management of ventricular and atrial arrhythmias associated with Brugada syndrome, HeartRhythm Case Rep. 4 (7) (2018) 270, https://doi.org/10.1016/j.hrcr.2018.01.008.
[8] M. Yavuz, T. Demircan, A potent ion channel blocker, hydroquinidine, exhibits strong anti-cancer activity on colon, pancreatic, and hepatocellular cancer cells, Mol. Biol. Rep. 50 (3) (2023) 2611–2621, https://doi.org/10.1007/s11033-023-08245-3.
[9] M. Yavuz, T. Demircan, Hydroquinidine demonstrates remarkable antineoplastic effects on non-small cell lung cancer cells, Curr. Mol. Med. 24 (9) (2024) 1159–1168, https://doi.org/10.2174/1566524023666230817115937.
[10] M. Yavuz, T. Demircan, The effect of hydroquinidine on proliferation and apoptosis of TMZ-Sensitive and -resistant GBM cells, Formerly as Curr. Med. Chem. Anti-Cancer Agents 23 (8) (2024) 938–952, https://doi.org/10.2174/1871520623666221125115542.
[11] T. Perrin, R. Guieu, L. Koutbi, F. Franceschi, J. Hourdain, M. Brignole, J.-C. Deharo, Theophylline as an adjunct to control malignant ventricular arrhythmia associated with early repolarization, Pacing Clin. Electrophysiol.: PACE (Pacing Clin. Electrophysiol.) 41 (5) (2018) 444–446, https://doi.org/10.1111/pace.13240.
[12] F. Angelini, S. Pourshayesteh, E. Gastino, M.M. Cingolani, D. Castagno, N. Cerrato, F. Gaita, G.M. De Ferrari, C. Giustetto, Long-term efficacy and safety of hydroquinidine in patients with Brugada syndrome, Eur. Heart J. 41 (Supplement_2) (2020), https://doi.org/10.1093/ehjci/ehaa946.0397 ehaa946.0397.
[13] B.L. Witt, T.O. Tollefsbol, Molecular, cellular, and technical aspects of breast cancer cell lines as a foundational tool in cancer research, Life 13 (12) (2023) 2311, https://doi.org/10.3390/life13122311.
[14] X. Dai, H. Cheng, Z. Bai, J. Li, Breast cancer cell line classification and its relevance with breast tumor subtyping, J. Cancer 8 (16) (2017) 3131–3141, https://doi.org/10.7150/jca.18457.
[15] Z. Huang, P. Yu, J. Tang, Characterization of triple-negative breast cancer MDA-MB-231 cell spheroid model, OncoTargets Ther. 13 (2020) 5395, https://doi.org/10.2147/OTT.S249756.
[16] O. Obidiro, G. Battogtokh, E.O. Akala, Triple negative breast cancer treatment options and limitations: future outlook, Pharmaceutics 15 (7) (2023) 1796, https://doi.org/10.3390/pharmaceutics15071796.
[17] M.C. Operti, A. Bernhardt, S. Grimm, A. Engel, C.G. Figdor, O. Tagit, PLGA-based nanomedicines manufacturing: technologies overview and challenges in industrial scale-up, Int. J. Pharm. 605 (2021) 120807, https://doi.org/10.1016/j.ijpharm.2021.120807.
[18] M.C. Operti, Y. Dölen, J. Keulen, E.A.W. van Dinther, C.G. Figdor, O. Tagit, Microfluidics-Assisted size tuning and biological evaluation of PLGA particles, Pharmaceutics 11 (11) (2019), https://doi.org/10.3390/pharmaceutics11110590. Article 11.

[19] M.C. Operti, D. Fecher, E.A.W. van Dinther, S. Grimm, R. Jaber, C.G. Figdor, O. Tagit, A comparative assessment of continuous production techniques to generate sub-micron size PLGA particles, Int. J. Pharm. 550 (1) (2018) 140–148, https://doi.org/10.1016/j.ijpharm.2018.08.044.
[20] M.C. Operti, A. Bernhardt, J. Pots, V. Sincari, E. Jager, S. Grimm, A. Engel, A. Benedikt, M. Hrubý, I.J.M. De Vries, C.G. Figdor, O. Tagit, Translating the manufacture of immunotherapeutic PLGA nanoparticles from lab to industrial scale: process transfer and in vitro testing, Pharmaceutics 14 (8) (2022), https://doi.org/10.3390/pharmaceutics14081690. Article 8.
[21] M.C. Operti, A. Bernhardt, V. Sincari, E. Jager, S. Grimm, A. Engel, M. Hruby, C. G. Figdor, O. Tagit, Industrial scale manufacturing and downstream processing of PLGA-based nanomedicines suitable for fully continuous operation, Pharmaceutics 14 (2) (2022), https://doi.org/10.3390/pharmaceutics14020276. Article 2.
[22] Y. Dölen, M. Valente, O. Tagit, E. Jäger, E.A.W. Van Dinther, N.K. van Riessen, M. Hruby, U. Gileadi, V. Cerundolo, C.G. Figdor, Nanovaccine administration route is critical to obtain pertinent init cell help for robust anti-tumor T and B cell responses, OncoImmunology 9 (1) (2020) 1738813, https://doi.org/10.1080/2162402X.2020.1738813.
[23] M. Bugnon, U.F. Röhrig, M. Goullieux, M.A.S. Perez, A. Daina, O. Michielin, V. Zoete, SwissDock 2024: major enhancements for small-molecule docking with attracting cavities and AutoDock Vina, Nucleic Acids Res. 52 (W1) (2024) W324–W332, https://doi.org/10.1093/nar/gkae300.
[24] J. Eberhardt, D. Santos-Martins, A.F. Tillack, S. Forli, AutoDock Vina 1.2.0: new docking methods, expanded force field, and python bindings, J. Chem. Inf. Model. 61 (8) (2021) 3891–3898, https://doi.org/10.1021/acs.jcim.1c00203.
[25] A. Daina, O. Michielin, V. Zoete, Swiss Target Prediction: updated data and new features for efficient prediction of protein targets of small molecules, Nucleic Acids Res. 47 (W1) (2019) W357–W364, https://doi.org/10.1093/nar/gkz382.
[26] G. Yu, L.-G. Wang, Y. Han, Q.-Y. He, clusterProfiler: an R package for comparing biological themes among gene clusters, OMICS A J. Integr. Biol. 16 (5) (2012) 284–287, https://doi.org/10.1089/omi.2011.0118.
[27] E. Trenkenschuh, W. Friess, Freeze-drying of nanoparticles: how to overcome colloidal instability by formulation and process optimization, Eur. J. Pharm. Biopharm. 165 (2021) 345–360, https://doi.org/10.1016/j.ejpb.2021.05.024.
[28] J. Wendorf, M. Singh, J. Chesko, J. Kazzaz, E. Soewanan, M. Ugozzoli, D. O'Hagan, A practical approach to the use of nanoparticles for vaccine delivery, J. Pharmaceut. Sci. 95 (12) (2006) 2738–2750, https://doi.org/10.1002/jps.20728.
[29] J.J.Y. Tan, J.B.L. Tan, Y.Y. Lim, Identification of bioactive cytotoxic compound of red button ginger extracted by solvent fractionation, J. Food Process. Preserv. 45 (2) (2021) e15125, https://doi.org/10.1111/jfpp.15125.
[30] M.A. Punke, P. Friederich, Amitriptyline is a potent blocker of human Kv1.1 and Kv7.2/7.3 channels, Anesth. Analg. 104 (5) (2007) 1256–1264, https://doi.org/10.1213/01.ane.0000260310.63117.a2, tables of contents.
[31] H. Pajouhesh, J.T. Beckley, A. Delwig, H.S. Hajare, G. Luu, D. Monteleone, X. Zhou, J. Ligutti, S. Amagasu, B.D. Moyer, D.C. Yeomans, J. Du Bois, J.V. Mulcahy, Discovery of a selective, state-independent inhibitor of NaV1.7 by modification of guanidinium toxins, Sci. Rep. 10 (1) (2020) 14791, https://doi.org/10.1038/s41598-020-71135-2.
[32] D. Aissaoui, S. Mlayah-Bellalouna, J. Jebali, Z. Abdelkafi-Koubaa, S. Souid, W. Moslah, H. Othman, J. Luis, M. ElAyeb, N. Marrakchi, K. Essafi-Benkhadir, N. Srairi-Abid, Functional role of Kv1.1 and Kv1.3 channels in the neoplastic progression steps of three cancer cell lines, elucidated by scorpion peptides, Int. J. Biol. Macromol. 111 (2018) 1146–1155, https://doi.org/10.1016/j.ijbiomac.2018.01.144.
[33] M. Bachmann, W. Li, M.J. Edwards, S.A. Ahmad, S. Patel, I. Szabo, E. Gulbins, Voltage-Gated potassium channels as regulators of cell death, Front. Cell Dev. Biol. 8 (2020), https://doi.org/10.3389/fcell.2020.611853.
[34] U. Banderali, M. Moreno, M. Martina, The elusive Nav1.7: from pain to cancer, in: S. Gentile (Ed.), Current Topics in Membranes, vol. 92, Academic Press, 2023, pp. 47–69, https://doi.org/10.1016/bs.ctm.2023.09.003.
[35] P. Pukkanasut, R. Jaskula-Sztul, J.C. Gomora, S.E. Velu, Therapeutic targeting of voltage-gated sodium channel NaV1.7 for cancer metastasis, Front. Pharmacol. 15 (2024), https://doi.org/10.3389/fphar.2024.1416705.
[36] A. Manzari-Tavakoli, A. Babajani, M.M. Tavakoli, F. Safaeinejad, A. Jafari, Integrating natural compounds and nanoparticle-based drug delivery systems: a novel strategy for enhanced efficacy and selectivity in cancer therapy, Cancer Med. 13 (5) (2024) e7010, https://doi.org/10.1002/cam4.7010.
[37] L.N. Al-Harbi, G.M. Al-Shammari, P. Subash-Babu, M.A. Mohammed, R. A. Alkreadees, A.E.A. Yagoub, Cinchona officinalis phytochemicals-loaded iron oxide nanoparticles induce cytotoxicity and stimulate apoptosis in MCF-7 human breast cancer cells, Nanomaterials 12 (19) (2022) 3393, https://doi.org/10.3390/nano12193393.
[38] W. Liu, Y. Qi, L. Liu, Y. Tang, J. Wei, L. Zhou, Suppression of tumor cell proliferation by quinine via the inhibition of the tumor necrosis factor receptor-associated factor 6-AKT interaction, Mol. Med. Rep. 14 (3) (2016) 2171–2179, https://doi.org/10.3892/mmr.2016.5492.
[39] J.S. Loh, L.K.S. Tan, W.L. Lee, L.C. Ming, C.W. How, J.B. Foo, N. Kifli, B.H. Goh, Y. S. Ong, Do lipid-based nanoparticles hold promise for advancing the clinical translation of anticancer alkaloids? Cancers 13 (21) (2021) 5346, https://doi.org/10.3390/cancers13215346.
[40] Q. Ru, X. Tian, M.-S. Pi, L. Chen, K. Yue, Q. Xiong, B.-M. Ma, C.-Y. Li, Voltage-gated K+ channel blocker quinidine inhibits proliferation and induces apoptosis by regulating expression of microRNAs in human glioma U87-MG cells, Int. J. Oncol. 46 (2) (2015) 833–840, https://doi.org/10.3892/ijo.2014.2777.
[41] C. Altamura, P. Gavazzo, M. Pusch, J.-F. Desaphy, Ion channel involvement in tumor drug resistance, J. Personalized Med. 12 (2) (2022) 210, https://doi.org/10.3390/jpm12020210.
[42] M. Li, P. Tian, Q. Zhao, X. Ma, Y. Zhang, Potassium channels: novel targets for tumor diagnosis and chemoresistance, Front. Oncol. 12 (2023), https://doi.org/10.3389/fonc.2022.1074469.
[43] L. Zúñiga, A. Cayo, W. González, C. Vilos, R. Zúñiga, Potassium channels as a target for cancer therapy: current perspectives, OncoTargets Ther. 15 (2022) 783, https://doi.org/10.2147/OTT.S326614.
[44] L. Leanza, P. O'Reilly, A. Doyle, E. Venturini, M. Zoratti, E. Szegezdi, I. Szabo, Correlation between potassium channel expression and sensitivity to drug-induced cell death in tumor cell lines, Curr. Pharm. Des. 20 (2) (2014) 189–200, https://doi.org/10.2174/13816128113199990032.
[45] I. El-Battrawy, J. Besler, X. Li, H. Lan, Z. Zhao, V. Liebe, M. Borggrefe, Impact of antiarrhythmic drugs on the outcome of short QT syndrome, Front. Pharmacol. 10 (2019) 771, https://doi.org/10.3389/fphar.2019.00771.
[46] L. Chen, Y. He, X. Wang, J. Ge, H. Li, Ventricular voltage-gated ion channels: detection, characteristics, mechanisms, and drug safety evaluation, Clin. Transl. Med. 11 (10) (2021) e530, https://doi.org/10.1002/ctm2.530.
[47] J. Iorio, I. Meattini, S. Bianchi, et al., hERG1 channel expression associates with molecular subtypes and prognosis in breast cancer, Cancer Cell Int. 18 (2018) 93, https://doi.org/10.1186/s12935-018-0592-1.
[48] A. Arcangeli, J. Iorio, C. Duranti, Targeting the hERG1 and β1 integrin complex for cancer treatment, Expert Opin. Ther. Targets 28 (3) (2024) 145–157, https://doi.org/10.1080/14728222.2024.2318449.
[49] A.A. Assiri, N. Mourad, M. Shao, P. Kiel, W. Liu, T.C. Skaar, B.R. Overholser, MicroRNA 362-3p reduces hERG-related current and inhibits breast cancer cells proliferation, Cancer Genom. Proteom. 16 (6) (2019) 433–442, https://doi.org/10.21873/cgp.20147.
[50] Q. Luo, T. Wu, W. Wu, G. Chen, X. Luo, L. Jiang, M. Deng, The functional role of voltage-gated sodium channel Nav1. 5 in metastatic breast cancer, Front. Pharmacol. 11 (2020) 1111, https://doi.org/10.3389/fphar.2020.01111.
[51] H. Rajaratinam, N.S. Rasudin, T.A.D. Al Astani, N.F. Mokhtar, M.M. Yahya, W. Z. Wan Zain, W.E. Mohd Fuad, Breast cancer therapy affects the expression of antineonatal Nav1. 5 antibodies in the serum of patients with breast cancer, Oncol. Lett. 21 (2) (2021) 108, https://doi.org/10.3892/ol.2020.12369.
[52] P. Pukkanasut, R. Jaskula-Sztul, J.C. Gomora, S.E. Velu, Therapeutic targeting of voltage-gated sodium channel NaV1. 7 for cancer metastasis, Front. Pharmacol. 15 (2024) 1416705, https://doi.org/10.3389/fphar.2024.1416705.
[53] L.M. Ballou, R.Z. Lin, I.S. Cohen, Control of cardiac repolarization by phosphoinositide 3-Kinase signaling to ion channels, Circ. Res. 116 (1) (2015) 127–137, https://doi.org/10.1161/CIRCRESAHA.116.303975.
[54] J. van der Horst, I.A. Greenwood, T.A. Jepps, Cyclic AMP-dependent regulation of Kv7 voltage-gated potassium channels, Front. Physiol. 11 (2020), https://doi.org/10.3389/fphys.2020.00727.
[55] W. Zhang, H.T. Liu, MAPK signal pathways in the regulation of cell proliferation in Mammalian cells, Cell Res. 12 (1) (2002) 9–18, https://doi.org/10.1038/sj.cr.7290105.
[56] N. Vasan, J. Baselga, D.M. Hyman, A view on drug resistance in cancer, Nature 575 (7782) (2019) 299–309, https://doi.org/10.1038/s41586-019-1730-1.